ACOUSTICS 2012

Numerical study of the aeroacoustic behavior of a subsonic confined cavity

P. Lafon[a], J. Berland[a], F. Crouzet[a], F. Daude[a] and C. Bailly[b]

[a]EDF R&D, 1 avenue du Général de Gaulle, 92141 Clamart, France
[b]Laboratoire de Mecanique des Fluides et d'Acoustique, 36 Av Guy de Collongue 69134 Ecully Cedex
philippe.lafon@edf.fr

Ducted cavities are typical configurations in pipe systems. They generate discrete tones which can be amplified by the coupling with the acoustic modes of the duct. This configuration has been numerically studied using high-order schemes and the physical phenomena have been retrieved. This paper presents a new step of this work in which different techniques for meshing the cavity are compared. The main goal is to validate approaches which are less restrictive for meshing industrial configurations.

1 Introduction

Ducted cavities are typical configurations in pipe systems with flow control devices such as valves. They generate discrete tones which can be amplified by the coupling with the acoustic modes of the duct. Like classical open cavities, ducted cavities underly a feedback mechanism that can be described as follows: vortical structures develop in the shear layer above the cavity and are convected downstream. The impact of the eddies on the downstream corner lead to pressure perturbations that trigger further instabilities at the upstream cavity corner giving a phase locking of the whole system, known as the Rossiter modes [1]. Additionally, in the ducted case, acoustic modes of the duct can also be excited. In the past, many experimental and numerical investigations about open cavities were done, especially for predicting resonance frequencies and pressure levels [2, 3].

The configuration considered here has been analysed in the context of an industrial application. It has been first studied in 2-D by using a second-order TVD-Euler code [4]. Rossiter frequencies were recovered and a cavity modification has been studied by introducing a chamfer at the upstream corner of the cavity which led to a reduction of the phenomena [5]. But turbulent aspects could not be considered due to the inviscid 2-D feature of the simulations. Then Navier-Stokes computations have been carried out on the same planar configuration but in 3-D. These computations have been performed using high-order methods and have retrieved more flow details [6]. This approach is continued in the present work but focusing on the meshing treatment of the cavity.

The computational algorithm involving low-dissipative and low-dispersive numerical methods is presented in the first section. In the second section, the studied configuration is presented with emphasis on experimental results and physical mechanisms. In the third section, the results obtained with two different grid treatments of the cavity are presented and analysed in order to characterize the different approaches able to deal with complex geometries.

2 Numerical algorithm

The set of equations are the compressible 3-D Navier-Stokes equations, written in conservative form after application of a general time-invariant curvilinear coordinates transformation from physical space to computational space. This transformation $(x, y, z) \rightarrow (\xi, \eta, \zeta)$ yields to a new expression for the Navier-Stokes equations:

$$\frac{\partial}{\partial t}\left(\frac{\mathbf{Q}}{J}\right) + \frac{\partial \mathbf{E}}{\partial \xi} + \frac{\partial \mathbf{F}}{\partial \eta} + \frac{\partial \mathbf{G}}{\partial \zeta} = 0,$$

where J is the Jacobian of the geometric transformation. The unknown vector writes $\mathbf{Q} = (\rho, \rho u, \rho v, \rho w, \rho e_t)^T$, where ρ designates the density, u, v, w the Cartesian velocity components and ρe_t the total energy. The latter is calculated for a perfect gas such as $\rho e_t = p/(\gamma - 1) + \frac{1}{2}\rho(u^2 + v^2 + w^2)$ with p the pressure. The flux vectors $\mathbf{E}$, $\mathbf{F}$, $\mathbf{G}$ contain the inviscid and the viscous terms. Their expressions as well as the metric identities for the grid transformation can be found in the literature [7, 8].

For interior points of the computational domain, the fluxes and the velocity derivatives for the viscous terms are discretized by standart 7-points or optimized 11-points centered finite difference schemes [9]. An explicit fourth-order low-storage Runge-Kutta scheme advances the solution in time. The CFL number is 0.9 and the time step Δt is updated every iteration during the transient phase. Appropriate 7-points or 11-points explicit low pass filters remove grid-to-grid oscillations, not resolved by centered finite difference schemes [9]. At the same time, the filters properly remove non-resolved turbulent structures and so act like a subgrid scale model. This method referred as LES-RF has been successfully applied in the literature [10, 11].

The finite difference schemes are limited to structured grids. In order to treat more complex geometries, a high-order overset capability has been implemented in the code. In this approach, the computational domain is subdivided into overlapping structured component grids. The governing equations are solved on each component grid separately and the communication between grids is achieved through interpolations. Also known as the Chimera grid method, this approach has been proposed first for aerodynamics [12] and extended later for aeroacoustic simulations [13]. For grid generation *Ogen*, the grid assembler module of the freely available library *Overture* [14] developed at the Lawrence Livermore National Laboratory, has been interfaced with the solver. For communication between grid boundaries that do not coincide, high-order interpolation is used. Lagrangian polynomials has been found to be best suited in terms of precision, execution time and implementation aspects for the high-order overset grid approach [15]. Various tests have shown that at least eighth-order polynomials have to be used in order to make the interpolation error negligible when using the 11-points scheme and fourth-order polynomials when using the 7-points scheme.

The standard Message Passing Interface (MPI) library routines have been used for code parallelization and, for load balancing purpose, each component grid is subdivided evenly N times in each direction and can be computed by $N_{\text{procs}} = N_{\xi,\text{procs}} \times N_{\eta,\text{procs}} \times N_{\zeta,\text{procs}}$..

All the aforementioned characteristics have been implemented in a numerical solver of the Navier-Stokes equations, called *Code_Safari* (Simulation of Aeroacoustic Flows And Resonance and Interaction). Details can be found in [16].

3 The case of the ducted cavity

Ducted cavities have been first studied for an industrial application: a whisthling phenomenon was observed on the power steam line of a nuclear power station [4]. A cavity

located in a gate valve was identified as the source of this pure tone.

It is well known that a flow past a cavity gives rise to noise radiation. A complex feedback process between the upstream and downstream corners produces coherent oscillations in the shear layer developing above the cavity [17, 18, 19]. For cavities in open space, the oscillations remain weak at low Mach numbers. Therefore most published papers are related to Mach number range in the high subsonic domain. For ducted cavities (see Figure 1), the possible coupling between hydrodynamic cavity oscillations modes and duct acoustic modes can lead to high amplitude oscillations even at low speeds. Cavity modes are given by Rossiter's formula [1]:

$$St_R = \frac{fd}{U_0} = \frac{n_R - \xi}{M_0 + U_0/U_c},$$

where $\xi = 0.25$, $U_0/U_c = 0.57$, and n_R is the mode number. The transverse modes of the duct are given by

$$St_d = f_d \frac{d}{U_0} = \frac{n_d\, c}{2H} \frac{d}{U_0},$$

where n_d is the duct mode number associated to the frequency f_d.

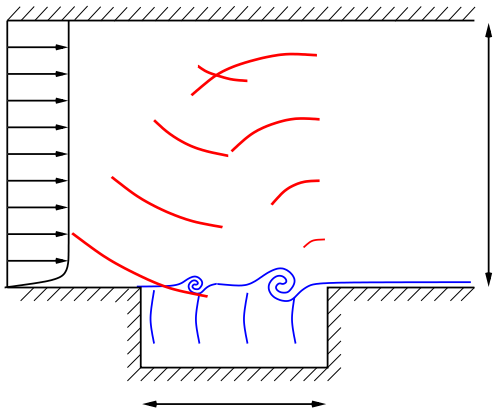

Figure 1: Hydrodynamic modes and acoustic modes in the ducted cavity configuration.

The real geometry of the industrial valve is quite complex and a simplified plane geometry was retained in order to study the physical phenomena. This cavity has two characteristics that are different from classical ones often considered in the literature: it is placed in a duct and it is partially covered. This geometry is displayed in Figure 2. The experimental results obtained in the previous studies [4, 20] are now used as validation data for the capability of numerical tools to capture the flow acoustic phenomena in such configuration.

In Figure 3, it is shown that the frequency of the cavity oscillation can lock-in the frequency of the pipe mode when Rossiter's mode approaches the duct mode. When lock-in occurs, the pressure level of the oscillations is maximum. At $M = 0.13$, the cavity mode 3 locks with the first transverse duct mode and at $M = 0.18$, the cavity mode 2 locks with the first transverse duct mode. At $M = 0.23$, the cavity mode 3 locks with the second transverse duct mode. More details about these results can be found in [6].

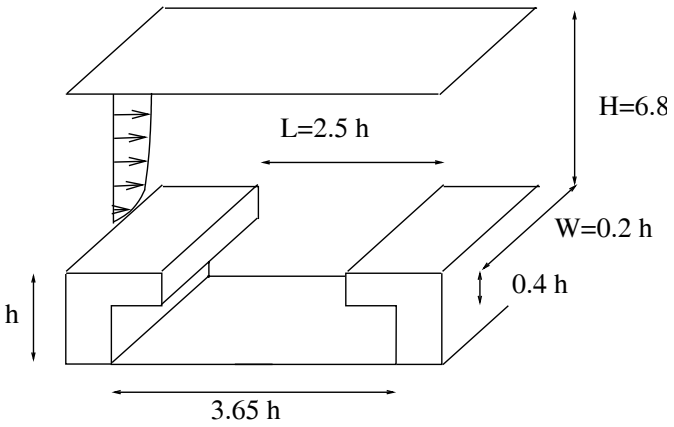

Figure 2: Sketch of the ducted cavity configuration.

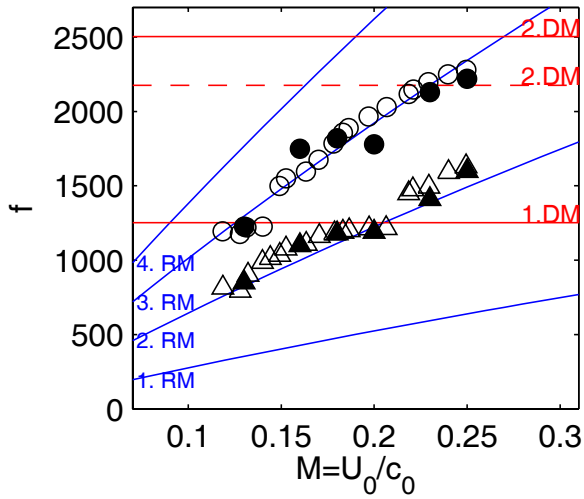

Figure 3: Computed frequencies (mode 2, ▲, mode 3, •) of the cavity modes compared to experimental ones (mode 2, △, mode 3, ○) and to Rossiter's and duct mode frequencies (RM = Rossiter's mode, DM = duct modes). The modified 2.DM mode is calculated with the sum of the duct and the cavity heights .

4 Tests for complex geometry treatments

4.1 Treatment of corners

It is well known that the shape of corners is a crucial point for the development of the physical phenomena and that a slight modification of this shape can modify the instability growth in the shear layer. These remarks are made for the cavity case but there are more or less valid for all cases of impinging shear layers where the shape of edges can be diverse.

The numerical treatment of these points depends on the discretization method that is choosen : finite volumes, finite difference, ... but it is also clear this numerical treatment is quite difficult: definition of a normal, expression of derivatives, ...

In our case, we have two solutions for the discretization of cavity corners:

- The first solution is to only consider component grids that are conformal (CG) and coincident. In this case, the situation of a unique structured grid is retrieved as it is shown in Figure 4. Then there is no numerical

errors introduced by the interpolation process. On the other hand, this approach appears to be quite restrictive as our final goal is to handle industrial configurations.

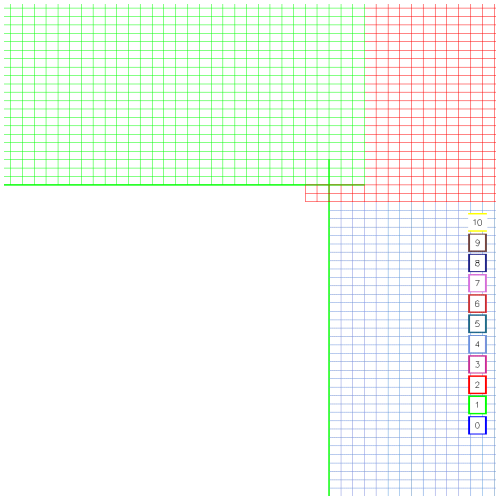

Figure 4: Zoom on the corner meshing with conformal grids (CG).

- The second solution is to introduce overlapping grids which are non-conformal (NCG). In this situation, corners are always treated as rounded edges. This is an approximation but it is a more versatile method able to give discretization solutions for more complex geometries while preserving the advantages of the numerical schemes. This situation is displayed in Figure 5. A curvilinear grid patch is superimposed on the other grids in order to build a rounded edge. This approach is of course much more flexible and it is now possible to introduce some geometry modifications to the cavity such as chamfers. This possibility is not studied here. Indeed, it is first necessary to study how it is possible to vary the radius of curvature of the rounded corner and to determine when it is equivalent to a sharp corner modelled with the first meshing method. In fact, two kinds of errors are now present : the modelling error due to the rounded edge and the interpolation error which is now present in the calculation contrary to the first approach. Figure 5 clearly displays the layers of interpolation points which make possible the communication between the grids.

4.2 Computational parameters

For the CG computation, 10 components grids are used for building the whole grid. For the NCG computation, an eleventh grid is added. For both cases, the total grid points is around 10 millions. For the CG computation, the minimum grid spacing is $\Delta x = 1. \times 10^{-4}$ m while for the NCG computation the minimum grid spacing is $\Delta x = 2. \times 10^{-5}$ m. As a consequence, the application of the CFL condition gives a time step of $\Delta t = 2. \times 10^{-7}$ s for the CG computation and of $\Delta t = 5.5 \times 10^{-8}$ s for the NCG computation.

It is well known that the boundary layer upstream the cavity plays a crucial role as its shape controls the vortex shedding and the convection of the eddies in the shear layer. In this work, the experimental boundary layer profile is fitted in

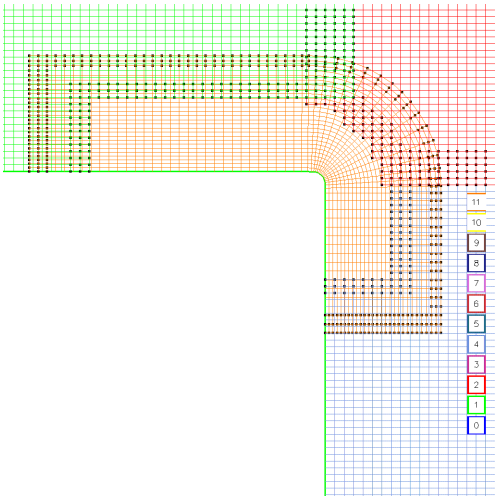

Figure 5: Zoom on the corner meshing with non-conformal grids (NCG).

a $1/n$ profile such as:

$$\frac{u_b(y)}{U_0} = \left(\frac{y}{\delta}\right)^{\frac{1}{n}},$$

where $\delta = 8.8$ mm and $n = 8.5$.

The upstream mean Mach number is $M_d = 0.20$ which corresponds to a maximum upstream Mach number $M_0 = 1.2 \times M_d = 0.24$.

This experimental profile is imposed as the initial condition and also as the inlet boundary condition. In order to preserve this profile till the cavity, a correction procedure is applied on the grids upstream the cavity (see [6] for details).

As the flow is in the low subsonic domain, the mean density and pressure are taken constant at the inflow and outflow. The Tam & Dong absorbing boundary condition is used for allowing acoustic waves to exit the computational domain. A sponge zone combining grid stretching and a Laplacian filter is applied at the outflow to avoid spurious reflections when eddies exit the computational domain.

4.3 Results

The figures 6 and 7 display two snapshots of the vorticity field for the conformal grid case and the non-conformal grid case, respectively. It seems that for the second case, the shear layer above the cavity develops more rapidly, showing bigger eddies. But, as the time step is much smaller for the NCG computation, the time duration of the calculation is still shorter and it is likely that the influence of the 2D coherent structures is still visible. This influence should decrease when the flow will switch to a full turbulent regime.

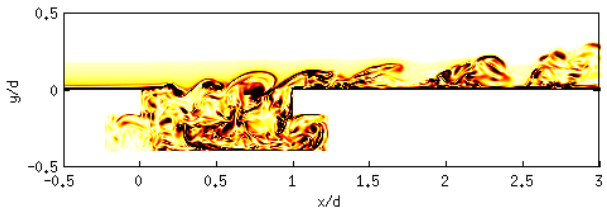

Figure 6: Snapshot of the vorticity field for conformal grids.

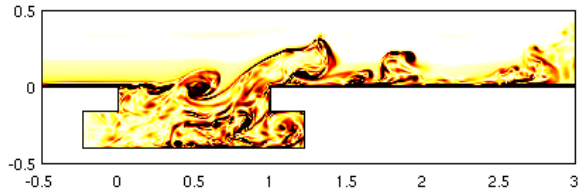

Figure 7: Snapshot of the vorticity field for non-conformal grids.

The figure 8 gives a comparison of the pressure spectrum for the two cases. It appears that the two computations retrieve the same phenomena except that the main peak is 4 dB lower for the NCG case. Then this is a quantitative difference that could be analysed through three main reasons:

- The curvature radius for the NCG case is too large to represent a sharp edge,
- There are some errors introduced by the presence of the interpolation points,
- As the time step is much smaller for the NCG computation, the duration of the pressure history used for obtaining the spectrum is not the same for the two cases. Further comparisons have to be carry out when the time duration of the two calculations will be equivalent.

The first and the two reasons given for explaining the differences between the two results seem the more plausible. In particular, a parametric study about the curvature ratio has to be done.

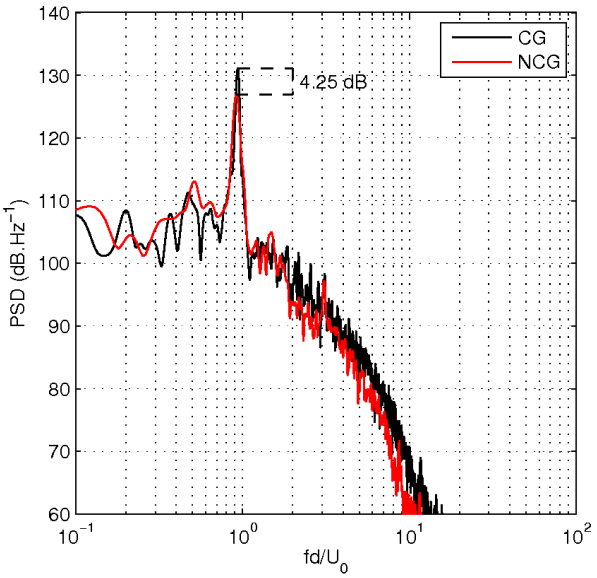

Figure 8: Pressure spectrum for conformal and non-conformal grids.

5 Conclusion

A high-order computational tool dedicated to aeroacoustic simulations, *Code_Safari*, has been apply to the case of a ducted cavity. The main goal of this work is to compare two main approaches for meshing the cavity and more precisely the upstream corner. It appears that the non-conformal grid technique which is the more flexible for complex geometries gives close results to the conformal grid technique. Nevertheless, a more detailed parametric study is necessary in order to obtain final results.

Acknowledgments

The authors wish to thank Dr Bill Henshaw (Lawrence Livermore National Laboratory) for his valuable recommendations concerning the overset-grid strategy.

References

[1] J. E. Rossiter. Wind-tunnel experiments on the flow over rectangular cavities at subsonic and transonic speeds. *Aeronautical Research Council Reports and Memoranda*, 3438, 1964.

[2] D. Rockwell and E. Naudascher. Self-sustained oscillations of impinging free shear layer. *Ann. Rev. Fluid Mech.*, 11:67–94, 1997.

[3] X. Gloerfelt, C. Bailly, and D. Juvé. Direct computation of the noise radiated by a subsonic cavity flow and application of integral methods. *J. Sound Vib.*, 266(1):119–146, 2003.

[4] P. Lafon, S. Caillaud, J. P. Devos, and C. Lambert. Aeroacoustical coupling in a ducted shallow cavity and fluid-structure effects on a steam line. *J. Fluids Struct.*, 18:695–713, 2003.

[5] P. Lafon and J. P. Devos. Computation of the noise generated by a shallow cavity and test of a solution for lowering the noise. *AIAA Paper*, 2003-3105.

[6] T. Emmert, P. Lafon, and C. Bailly. Numerical study of aeroacoustic coupling in a subsonic confined cavity. *AIAA Paper*, 2008-2848.

[7] M. R. Visbal and D. V. Gaitonde. On the use of higher-order finite-difference schemes on curvilinear and deforming meshes. *J. Comput. Phys.*, 181:155–185, 2002.

[8] O. Marsden, C. Bogey, and C. Bailly. High-order curvilinear simulations of flows around non-cartesian bodies. *J. Comput. Acous.*, 13(4):732–748, 2005.

[9] C. Bogey and C. Bailly. A family of low dispersive and low dissipative schemes for large eddy simulations and for sound propagation. *J. Comput. Phys.*, 194(1):194–214, 2004.

[10] D. V. Gaitonde and M. R. Visbal. Advances in the application of high-order techniques in simulation of multidisciplinary phenomena. *International Journal of Computational Fluid Dynamics*, 17:95–106, 2003.

[11] C. Bogey and C. Bailly. Turbulence and energy budget in a self-preserving round jet: direct evaluation using large-eddy simulation. *J. Fluid Mech.*, 627:129–160, 2009.

[12] J. A. Benek, J. L. Steger, and F. C. Dougherty. A flexible grid embedding technique with applications to the Euler equations. *AIAA Paper*, 1983-1944.

[13] J.W. Delfs. An overlapped grid technique for high resolution CAA schemes for complex geometries. *AIAA Paper*, 2001-2199.

[14] W. D. Henshaw. Ogen: an overlapping grid generator for overture, tech. rep. ucrl-ma-132237. Technical report, Lawrence Livermore National Laboratory, 1998.

[15] S. E. Sherer and J. N. Scott. High-order compact finite-difference methods on general overset grids. *J. Comput. Phys.*, 210:459–496, 2005.

[16] F. Daude, J. Berland, T. Emmert, P. Lafon, F. Crouzet, and C. Bailly. A high-order finite-difference algorithm for direct computation of aerodynamic sound. *Computers and Fluids*, In press, 2011.

[17] D. Rockwell. Oscillations of impinging shear layers. *AIAA Journal*, 21:645–664, 1983.

[18] C. M. Shieh and P. J. Morris. Parallel computational aeroacoustic simulation of turbulent subsonic cavity flow. *AIAA Paper*, 2000-1914.

[19] X. Gloerfelt, C. Bogey, and C. Bailly. Numerical evidence of mode switching in the flow-induced oscillations by a cavity. *Int. J. of Aeroacoustics*, 2(2):193–218, 2003.

[20] X. Amandolese, P. Hemon, and C. Regardin. Study of the acoustic oscillations by flows over cavities. Part 1. internals flows. *Proceedings of the Fifth International Symposium on Fluid-Structure Interactions, IMECE'02, New Orleans*, 2002.